TECHNICAL UNIVERSITY OF CLUJ-NAPOCA

ACTA TECHNICA NAPOCENSIS

Series: Applied Mathematics, Mechanics, and Engineering
Vol. 65, Issue Special I, February, 2022

A FUNCTIONAL DESIGN ANALYSIS FOR A ROBOTIC GUIDED INSTRUMENT USED IN RADIOFREQUENCY ABLATION

Andrei CĂPRARIU, Nadim Al HAJJAR , Calin VAIDA, Florin GRAUR, Adrian PÎSLĂ, Emil MOIȘ, Paul TUCAN, Corina RADU, Iosif BIRLESCU, Doina PÎSLĂ

Abstract: *The paper presents the design improvement of a medical instrument used for a robotic-assisted radiofrequency ablation (RFA). In the first part, the requirements of the device have been pointed out, and then, the prototype of the device has been analyzed and its weaknesses have been identified. Some finite element simulations have been achieved to test the mechanical strength of the device in various conditions. Based on the derived numerical data, the study shows the specific optimization parameters for the device, which can be improved without changing its general structure*
Key words: *Robotic-assisted RFA, robotic instrument, CAD, FEM, optimization.*

1. INTRODUCTION

According to World Health Organization (WHO), "Cancer is a generic term for a large group of diseases that can affect any part of the body" [1]. In 2020, liver cancer was the third most common cancer-related causes of death, with around 830 000 deaths worldwide [1]. The most common type of primary liver cancer is Hepatocellular Carcinoma (HCC) (80-90% of the cases). HCC is followed by Cholangiocarcinoma (CCA) (10-15% of the cases) [2]. However, metastatic (secondary) liver cancer is 18 to 40 times more common than primary liver cancer [2] due to the anatomic position of the liver.

The preferred HCC treatment methods are surgical resection and liver transplant [3- 5]. However, most of the patients are unable to withstand surgery (resection) due to various conditions such as cirrhosis [6]. The transplantation can be performed when there is only one lesion, smaller than 50 mm or up to 3 lesions, each smaller than 30 mm. Furthermore, liver transplantation is not available in all countries, and the number of available donators is insufficient [3]. When surgery cannot be performed, several other therapies are available. The injection of absolute ethanol is an easy to perform method with few side effects, with good results for the patients who cannot tolerate surgery and for the cases of recurrent HCC. The method is limited for tumors smaller than 40 mm [6] [7]. Transcatheter arterial chemoembolization (TACE) is another method, mostly used for shrinking tumors and for intermediate stages of HCC [6]. Another widely used method is systemic chemotherapy which is less efficient than regional chemotherapy [8]. Radiofrequency ablation (RFA) is a technique with good efficiency for patients with early-stage HCC. The method allows the complete ablation of the liver tumors in only one or two sessions. The radiofrequency ablation method uses the heat generated from medium frequency alternating current to ablate the tumor [6]. The procedure can be achieved by using a special needle containing electrodes inserted into the tumor and can deliver a specific dose of electromagnetic radiation [9].

The main limitations of RFA are correlated to the precision of the needle insertion. The precision may vary based on the tumor location, surgeon experience, and the medical imaging accuracy. To circumvent the accuracy and possible ergonomics challenges of RFA, robotic systems may be used, mainly in the needle insertion stage [15]. Several robotic systems for

RFA were used in medical practice, such as ROBIO [8] and MAXIO [9]. In [10], the authors presented an automated RFA needle insertion instrument that was designed to be compatible as an end-effector of a medical robotic system (e.g., PARA-BRACHYROB [12]) which was tested in laboratory conditions. According to the experimental data, several drawbacks were identified for the RFA instrument. The main goal of this paper is to describe the study regarding the RFA instrument optimization, which is conducted using various finite element analysis (FEA) methods.

The paper is structured as follows: Section 2 presents the RFA instrument focusing on its main components; Section 3 describes the main requirements of the RFA instruments; Section 4 presents a detailed design analysis; Section 5 describes a strength improvement analysis, and the conclusions are drawn in Section 6.

2. RFA INSTRUMENT DESCRIPTION

An instrument for the robotic-assisted percutaneous RFA procedure was developed at the Technical University of Cluj-Napoca [10, 12, 14, 16]. Figure 1 presents the first experimental model of the RFA instrument, in the home position (needle fully retracted).

The instrument is composed of three main modules: Base, Insertion, and Opening, according to figures 3,4 and 5. The Base module is the fixed one and it is attached to the robot. The Insertion module is designed for needle insertion (into the tumor). Finally, the Opening module is designed to push the electrodes handle (of the ablation probe), which in turn opens (inserts) the electrodes within the tumor. The insertion module is sliding on the base module, whereas the opening module is sliding on the insertion module. Figure 2 presents the ablation probe in 3 different positions: A – electrodes closed; B – electrodes at the first insertion level; C – electrodes at the last insertion level.

The main components of the base module are presented in Figure 3.Component 1 is the cone to guide the ablation needle during the procedure by minimizing needle bending. The two tips of the insertion mechanism's lead screw are mounted inside two bearings.

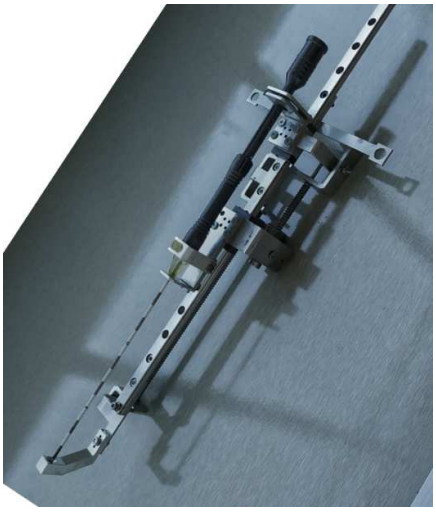

Fig. 1. RFA Instrument – first experimental model

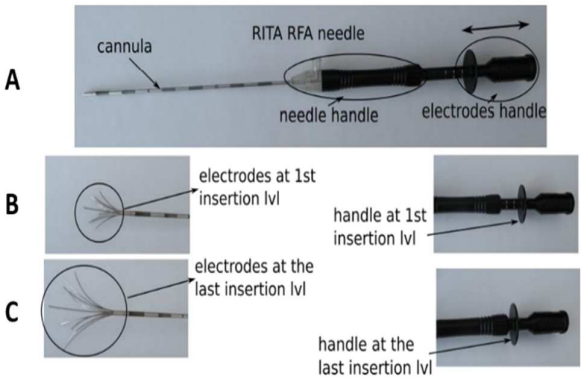

Fig. 2. RFA Probe [8].

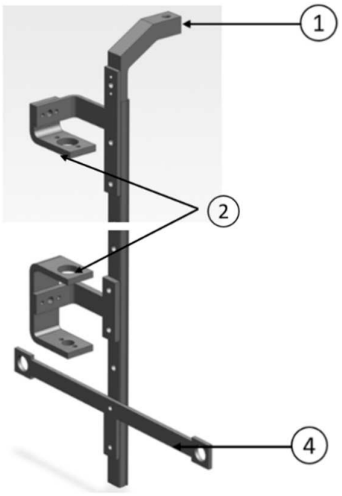

Fig. 3. Base Module – Components

The two bearings are fixed in components 2. Component 3 is the translation rail. Both insertion and opening mechanisms are sliding along the rail. Component 4 is the fixation part of the entire device.

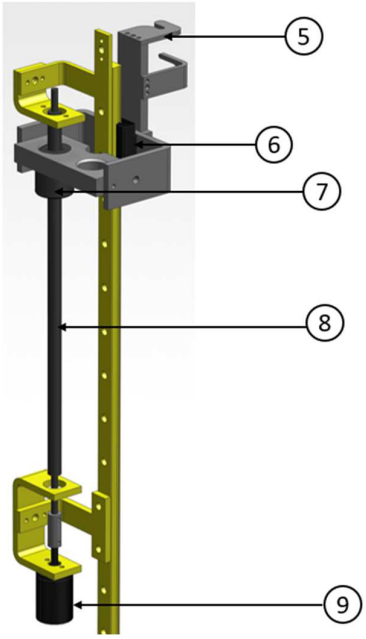

Fig. 4. Insertion Module - Components

Figure 4 present the insertion module, isolated from the entire device, along with its main components. The needle handle is attached to the device by Component 5. Component 6 is the slider of the insertion mechanism. Component 7 is the nut of the insertion mechanism, and the leadscrew is component 8. The insertion mechanism is actuated by Motor 9. The yellow-colored components from Figure 4 belong to the base module.

Figure 5 presents the opening module, isolated from the rest of the device. The leadscrew of the opening mechanism is Component 10, and the nut is Component 11. The Opening module is actuated by motor 13. The electrodes handle is attached to component 12. The yellow parts belong to the base module and the red ones to the insertion module.

For the needle insertion/retraction, Motor 9 is rotating Screw 8, and the rotation of the Screw 8 is converted into translation by the leadscrew-nut mechanism (composed of Screw 8 and Nut 7). Because Nut 7 is bounded to Slider 6, the slider will translate along Rail 3 together with the needle handle. Since the opening module is fixed on the insertion module, the translation will also be imposed on the opening mechanism. After the needle insertion, the tip needle should open. This is achieved by Motor 13 which rotates the leadscrew of the opening mechanism – 10. The rotation of Screw-10 will cause the translation of the Nut-11, which will move the slider together with the electrodes handle.

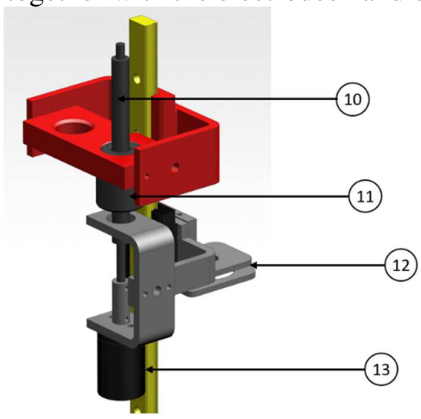

Fig. 5. Opening Module – Components

3. SYSTEM REQUIREMENTS

The first step in the design improvement of the RFA instrument is the identification of the requirements. The requirements are listed and classified in Table 1.

Table 1

RFA instrument requirements

Type	Symbol	Requirement
Main Requirement	**M-01**	The device must perform the RFA procedure
Functional Requirements	**F-01**	The device should be able to insert/retract the RFA probe
	F-02	The device should be able to open/close the tip of the RFA probe
	F-03	The device should be able to hold the RFA probe
	F-04	The device should be remote controlled by the user
	F-05	The device should not allow the probe retraction while the electrodes are opened
Performance Requirements	**P-01**	The device should be able to provide the insertion force of maximum 14 N
	P-02	The device should be able to provide the insertion velocity of 25-40 mm/s

	P-03	The device should be able to provide the probe opening force of maximum 20 N
	P-04	The device should be able to provide the probe opening velocity of minimum 10 mm/s
	P-05	The device should be able to provide the insertion precision of 0.1 mm
	P-06	The device should be able to measure the insertion force in X, Y and Z with the precision of 0.1 N
Usability Requirements	**U-01**	The device should be easy to use for a person with a medical training
	U-02	The control interface of the device should be easy to use
	U-03	The usage of the device should be easy to learn, and easy to remember how to use it
	U-04	The user of the device should not be required to consult the manual each time is using the device
	U-05	The usage of the device should not require a very advanced training
Interface Requirements	**I-01**	The device should be able to be held by a serial or parallel robot with the payload of 1 kg
	I-02	The device should not harm the patient
	I-03	The device should not harm its user
	I-04	The device should not deteriorate any surrendering equipment
	I-05	The device should provide the connection of the RFA probe to the radiation source
	I-06	The device should provide the connection of the RFA probe to the anesthetic source
	I-07	The input and output wires and pipelines of the device should not get entangled with any equipment
	I-08	The device should have a user-friendly design
	I-09	The device should be able to connect to the power supply of the hospital
	I-10	The noise produced by the device should be under 80 dB
Modes and/or States Requirements	**S-01**	The device should be able to operate in a manual mode
	S-02	The device should be able to operate in automatic mode
	S-03	The device should be able to operate in a troubleshooting and maintenance mode
	S-04	The device should have the emergency stop" hardware function
Adaptability Requirements	**A-01**	The device should be able to be mounted on a multitude of serial robots with the payload greater than 1kg
	A-02	The device should be able to be mounted on a multitude of parallel robots with the payload greater than 1 kg
	A-3	The device should be modular, so more features could be added in the future
Physical Constraints	**B-01**	Maximum X dimension: 200mm
	B-02	Maximum dimension: 200mm
	B-03	Maximum Z dimension: 400mm
	B-04	Maximum weight: 800 g
Design Constraints	**D-01**	The device should be constructed of inorganic and resistant to water, dilute acids and alkalis, solvents, disinfectants and decontamination agents materials
	D-02	The device should have measures to drain accumulated electric charges from all nonconductive surfaces to avoid electrostatic discharging
	D-03	The device should be constructed of environment-friendly materials
Environmental Conditions	**E-01**	The device should be able to operate in an ISO5 cleanroom environment (ISO 14644-1)
	E-02	The device should be sterilizable to SAL6 and maintained at this level throughout operations.
	E-03	The device should be able to properly operate in room with the temperature between 10 and 40 °C
	E-04	The device should be able to properly operate in room with the maximum humidity level of 70&
Logistical Requirements	**L-01**	Maintenance and verification of the device should be performed on regular basis
	L-02	The spare parts of the device should be easy to find and replace
	L-03	The transportation of the device should be safe, without the risk of deterioration
	L-04	The technical documentation of the device should be clear and easy to understand
	L-05	The implementation time of the device should be short

	L-06	The device should be easy to implement
	L-07	The device should be easy to calibrate
Policies and Regulations	**R-01**	The device should be designed to respect the IEC 80601-2-77:2019 Quality Standards
	R-02	The device should be designed to respect the IEC 80601-2-77:2019 Safety Standard

4. DETAILED DESIGN ANALYSIS

After defining the system's requirements, the original RFA instrument was analyzed, and its weaknesses were identified. This section presents the description of the identified weaknesses. The weaknesses of the RFA automated instrument can be classified into three main categories: design weaknesses, manufacturing errors, and mechanical strength weaknesses.

4.1. Design Weaknesses

This category mainly refers to some features that were not present or not properly designed in the initial state and is further subcategorized as:
Inappropriate attachment of the RFA probe on the device.
Inappropriate bearing fixation.
Inappropriate cone support.
Figure 6 presents the ablation probe attached to the instrument where the three attachment areas are highlighted. In the current configuration, the needle has to be bent in order to be attached to the device. The maximum distance between the attachment points 1 and 3 is shorter than an optimum value. Figure 7 presents how the probe is currently attached on the device. The first step of the RFA probe attachment is the insertion of the needle into the cone (area 3). In the current configuration, in this step, the needle has to be bent. The second step is pushing the probe in area 1 and area 2. The tips of the leadscrews are mounted inside ball bearings. In the current configuration, the bearings are not locked against axial displacement.
The axial forces produced by the device are pushing the bearings out of their fixing holes. Figure 8 presents the inappropriate fixation of the bearings.

The reaming of the cone of which should offer radial support to the needle during the ablation procedure, is too large.

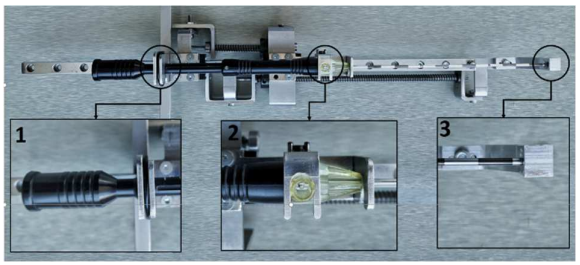

Fig. 6. RFA probe attachment

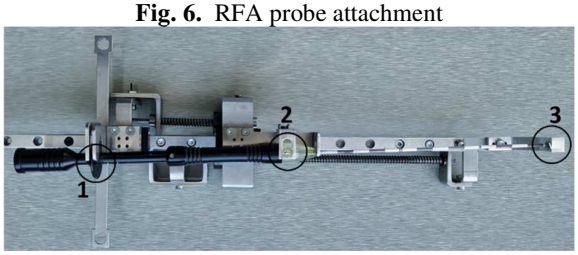

Fig. 7. RFA probe - Inappropriate Attachment

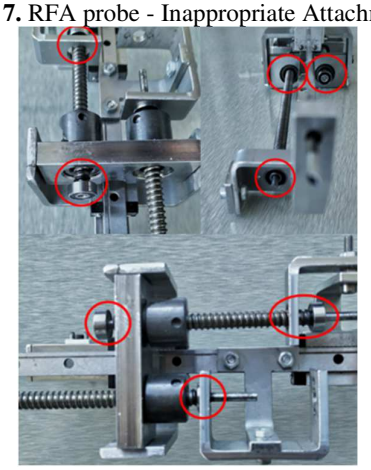

Fig. 8. Inappropriate Bearing Fixation

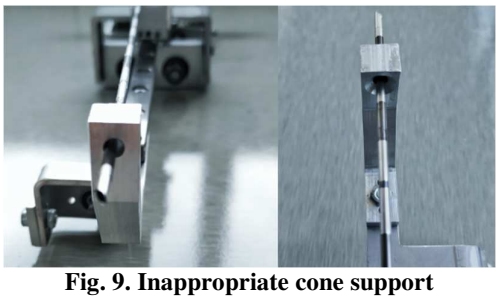

Fig. 9. Inappropriate cone support

Inappropriate radial support affects the precision of the ablation, produces higher vibration and buckling of the needle. Figure 9 presents the needle inside the cone.

4.2. Manufacturing errors

Some of the structural components of the device are manufactured through the bending procedure which does not ensure the required precision. Figure 10 presents some angles that are visibly not perpendicular.

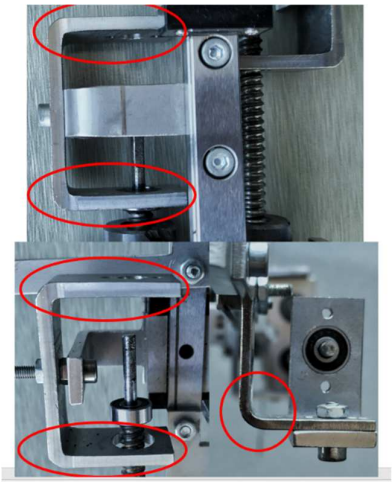

Fig. 10. Execution Anomalies

4.3. Mechanical strength weaknesses

In order to test the mechanical resistance of the structural components of the device, four finite element (FEM) simulations have been performed.

End of Stroke - Insertion Module Simulation. The first FEM analysis simulates a case when the insertion module is positioned at the end of its stroke and the motor is further actuated. Figure 11 presents the load case scenario of the simulation. The insertion module is positioned at the end of its stroke as if the needle is fully inserted. The opening module is positioned at the beginning of its stroke as if the ablation probe is completely closed.

A boundary condition - fixed DOF:123456 is applied on the holes of the attachment component as if the device is mounted on a robot.

As Figure 12 presents, the end of the stroke of the insertion module is limited by the highlighted screw, which doesn't allow the slider to continue the translation in the +Z direction. In the simulation, a boundary condition was applied on the slider's facet - fixed DOF:3.

For simulation convergence reasons, an additional boundary condition - fixed DOF123456 was applied on the tip of the device.

In previous experiments, it was measured that the maximum insertion force was 14 N [8]. For this simulation, a safety coefficient of 1.5 was applied; therefore, the applied force is 21 N.

The 21 N load was applied on the interior nodes of the insertion module's lead screws mechanism's nut.

Figure 13 presents the overall stress results of the first simulation at the full load state. The colored scale measures the von Mises stress in MPa. The upper value of the scale represents the Yield strength of the material the device is constructed of - 310 MPa.

Since the von Mises stress of components C1, C2 and C3 exceeded the Yield strength limit, the reinforcement of those components is required

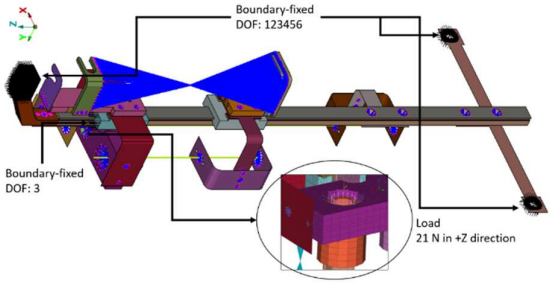

Fig. 11. End of Stroke Insertion – Load Case

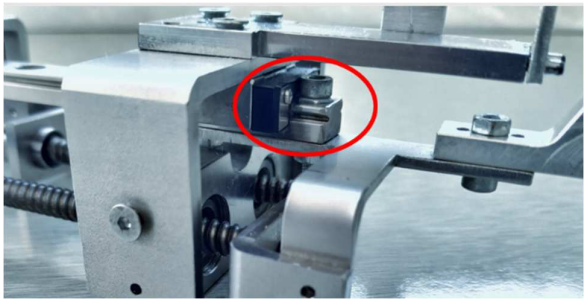

Fig. 12. Insertion Module - End of Stroke Limitation

Blocked Insertion Simulation. The second simulation is also testing the strength of the insertion module. It simulates the case when the insertion module is positioned at the beginning of its stroke, but the probe is not able to translate, and the motor is further actuating the module.

Figure 14 presents the load case scenario of the simulation. The insertion module is positioned at the beginning of the insertion position. The

opening module is also positioned at the beginning of its stroke as if the ablation probe is completely closed. A boundary condition - fixed DOF123456 is applied to the holes of the fixation component of the device as if the device is mounted on a robot.

For simulation convergence reasons, an additional boundary condition - fixed DOF123456 was applied on the tip of the device.

In the case when the insertion of the needle is blocked, the support component of the fixed part of the probe will not be able to move in the +Z direction.

A boundary condition – DOF 3 will limit the translation of the fixed support component in the +Z direction.

The same 21 N force in the +Z direction is applied on the nut of the insertion module's lead-screw mechanism.

Figure 15 presents the overall stress results of the Blocked Insertion simulation at the full load state. The scale from the picture measures the von Mises stress in MPa

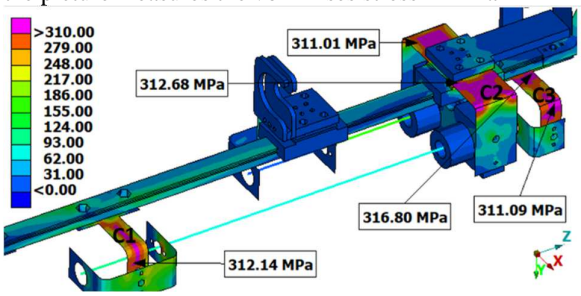

Fig. 13. Insertion Module - End of Stroke von Mises stress

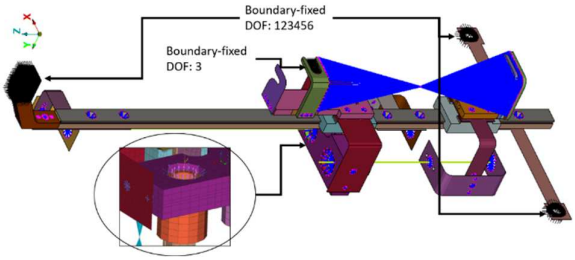

Fig. 14. Blocked Insertion Simulation – Load case

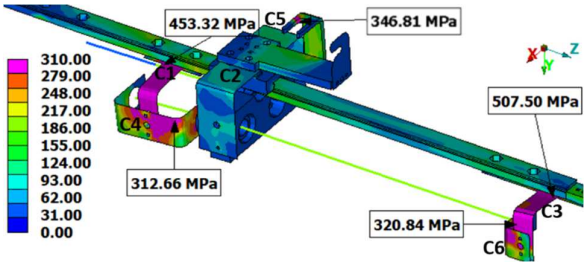

Fig. 15. Blocked Insertion - von Mises stress

Compared to the first simulations, the von Mises stresses of components C1 and C3 are higher in the second simulation, and the stress of component C2 is lower. Additionally, two more components exceeded the Yield strength limit: C4, C5, and C6.

Since the von Mises stress of components C4, C5 and C6 exceeded the Yield strength limit, those should also be reinforced for avoiding their plastic deformation during the use of the device.

End of Stroke – Opening Module Simulation. The third simulation tests the strength of the opening module in the case when the module is positioned at the end of its stroke and the motor is further pushing it. Figure 16 presents the load case scenario of the simulation. The insertion module is positioned at the end of its stroke as if the needle is fully inserted. The opening module is also positioned at the end of its stroke as if the ablation probe is completely opened. The boundary conditions are similar to the ones from the first simulation.

In previous laboratory experiments, the maximum opening force was measured to be around 20 N. For this simulation, a safety coefficient of 1.5 was applied, so the opening force is 30 N.

A 30 N force in the +Z direction is applied on the nut of the opening module's lead-screw mechanism. The translation of the opening module is blocked by the contact between the nut and the motor support component. Figure 17 presents the overall stress results of the End of Stroke - Tip Opening simulation at the full load state. The scale from the picture measures the von Mises stress in MPa

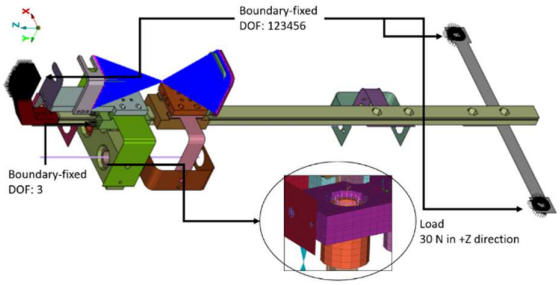

Fig. 16. End of Stroke - Opening Simulation – Load Case

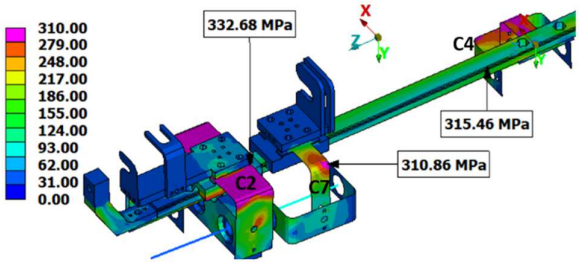

Fig. 17. Opening Module - End of Stroke Simulation – von Mises stress

In this simulation, higher stresses were noticed on components C2 and C4 compared to the previous two simulations. Additionally, component C7 exceeded the yield strength limit. According to the result of the simulation, component C7 should also be redesigned.

Blocked Tip Opening Simulation. The fourth simulation is also testing the strength of the tip opening module. It simulates the case when the opening module is positioned at the beginning of its stroke, but the probe is not able to open, and the motor is further actuating the module. Figure 18 presents the load case scenario of the simulation. The insertion module is positioned at the end of its stroke. The opening module is positioned at the beginning of its stroke as if the ablation probe is completely closed. A boundary condition - fixed DOF123456 is applied to the holes of the fixation component of the device as if the device is mounted on a robot. For simulation convergence reasons, an additional boundary condition - fixed DOF123456 is applied on the tip of the device.

The insertion module's motion in the Z direction is constrained using a boundary condition - fixed DOF 3 on the front facet of the slider. In the case when the probe is not able to open, the support component of the mobile part of the probe will not be able to move in the +Z direction. A boundary condition – DOF 3 will limit the translation of the mobile support component in the +Z direction. The same 30 N force in the +Z direction is applied on the nut of the insertion module's lead-screw mechanism. Figure 19 presents the overall stress results of the Blocked Tip Opening simulation at the full load state. The scale from the picture measures the von Mises stress in MPa. In the fourth simulation, a slightly higher stress was noticed on component C7 compared to the previous simulations

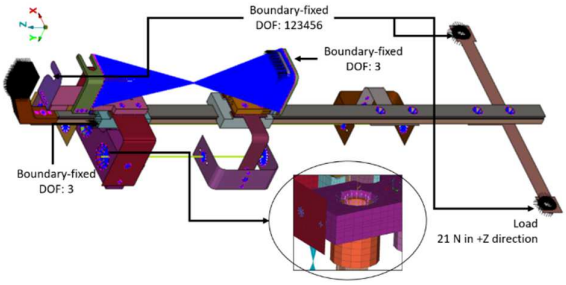

Fig. 18. Blocked Opening – Load Case

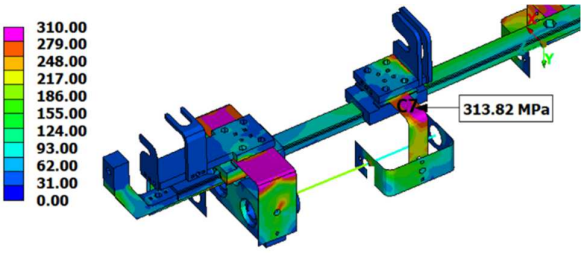

Fig. 19. Blocked Opening Simulation – von Mises stress

Table 2 presents the overall results of the previous simulations. For components C1, C3, C5, and C6, the highest stresses were produced in the second simulation - Blocked Insertion. For components C2 and C4, the highest stresses were noticed in the third simulation -End of Stroke – Opening Module Simulation. The worst stress for component C7 was noticed in the fourth simulation - Blocked Opening, where the maximum stress was less than 3 MPa higher than the stress from the third simulation. The deformation shapes were similar for each component in the four simulations

Table 2

Results of the FEM simulations

Component	Maximum von Mises stress [MPa]	Simulation
C1	312.14	SIM1
	453.32	**SIM2**
	311.1	SIM3

	321.65	SIM4
C2	312.68	SIM1
	332.68	**SIM3**
	323.06	SIM4
C3	316.8	SIM1
	507.5	**SIM2**
	357.24	SIM3
	325.82	SIM4
C4	312.66	SIM2
	315.46	**SIM3**
C5	346.81	**SIM2**
C6	320.84	**SIM2**
C7	310.86	SIM3
	313.82	**SIM4**

5. STRENGTH IMPROVEMENT ANALYSIS

As seen in the CAE simulations, (Figure 13, Figure 15, Figure 17, Figure 19) the stress of the seven identified components: C1, C2, C3, C5, C6, and C7 exceeded the yield limit. This chapter presents the redesign of the instrument, to reduce the stresses of the seven components as close as possible or under the yield limit without modifying the general shape of the components. The deformation shape of each of the seven components was the starting point of the redesign. The components were modified directly in the FEM pre-processor. Based on the preliminary result of the modifications, the device will be optimized in CAD software, and the new solution is analyzed again.

For reinforcing component C1, its thickness was increased from 3 mm to 5 mm. Also, its shape was slightly modified, as presented in Figure 20. The two facets were moved to the interior to compensate for the increased thickness.

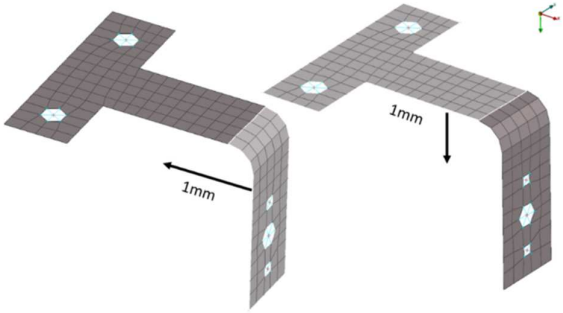

Fig. 20. Component C1 modification

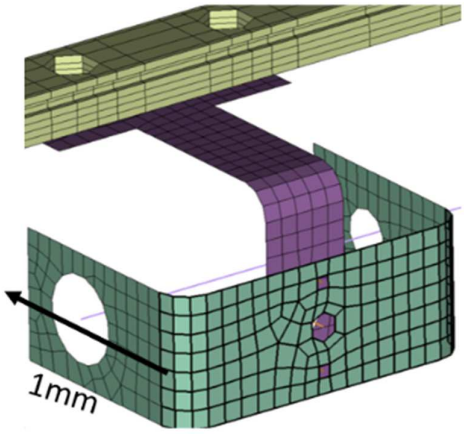

Fig. 21. Component C4 modification

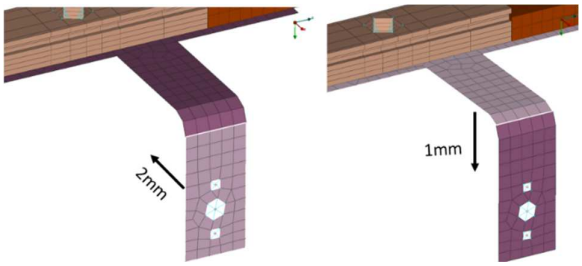

Fig. 22. Component C3 modification

The redesign of component C1 imposed a slight shape modification of component C4, as presented in Figure 21. The thickness of component C3 was increased from 2 mm to 4 mm. Figure 22 presents the modifications of component C3. To reduce the torsion of the upper facet from the figure, the side facet was moved 2 mm in the interior. The upper facet was also moved 1 mm to the interior. The redesign of component C3 imposed a slight shape modification of component C6.

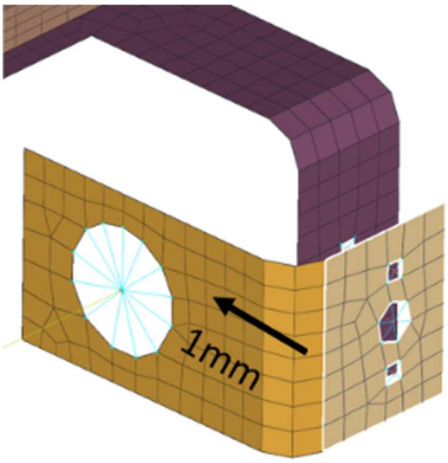

Fig. 23. Component C6 modification

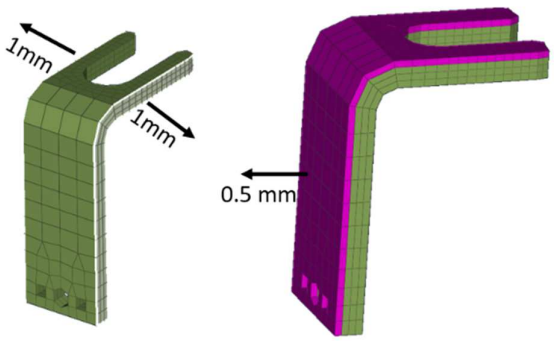

Fig. 24. Component C5 modification

As presented in Figure 23, the side facet was moved 1 mm in the interior. The previously presented modifications have the potential to reduce the stresses on C2 and C7. In this case, components C2 and C7 were not modified. Component C5 was thickened as shown in Figure 24: 1 mm added on each side facet and 0.5 mm added on the top facet.

As discussed before, the second and the third simulations were the ones that induced the highest stresses in the model. Those two simulations were repeated for the redesigned device.

Figure 25 presents the stresses of components C1, C3, C5 and C6 in the second simulation. The top of the picture presents the components from the initial device and the bottom of the picture presents the components from the redesigned device. Figure 26 presents the stresses of components C2, C4, and C7 in the third simulation. The improvement of components C1, C3, C5 and C7 is significant one. The stresses for the other three key components, C2, C4 and C6 is slightly reduced. The overall stresses of the device are reduced in the redesigned device

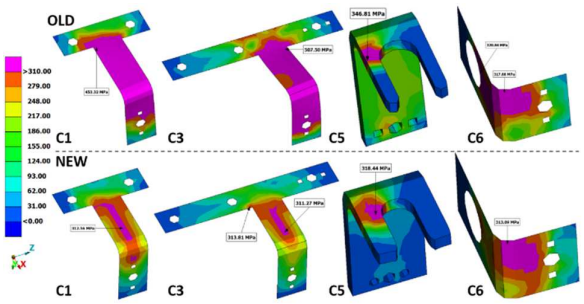

Fig. 25. SIM2 - New Results

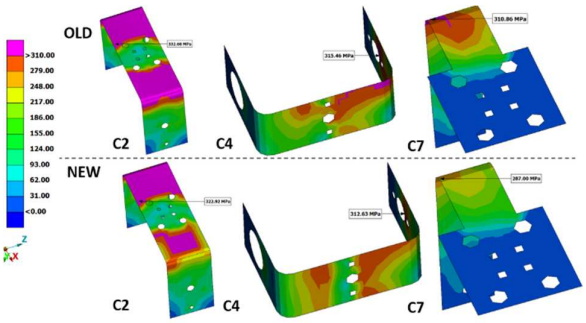

Fig. 26. SIM3- New Results

The results of the new simulation are showing that the mechanical strength of the instrument can be easily improved. As a consequence, changing the general structure of the instrument is not required for solving the identified problems.

In order to fix the inappropriate attachment of the RFA probe, the distance between the attachment points of the probe will be increased within the imposed limits. The inappropriate bearing fixation problem will be solved by thickening the components where the bearings are fixed and providing axial support. Thickening those components is also demonstrated to be a solution for strength improvement. The inappropriate cone support problem will be solved by mounting some rubber dampers inside the cone. The execution weaknesses will be solved by rebuilding the structural components on more precise machines and, if needed, using the milling procedure instead of the bending procedure.

6. CONCLUSIONS AND FURTHER DIRECTIONS

Although various HCC treatment procedures are available nowadays, the mortality of the disease is still at a high level.

This paper presented a functional analysis of an instrument for robotic guided RFA treatment for HCC, resulting in a set of improvement solutions of a medical instrument used for the robotic-assisted RFA. The design, manufacturing, and mechanical strength weaknesses of the prototype of the device have been identified and analyzed.

The results of the analysis showed that the instrument can be easily improved without changing its general structure.
Further work is required for achieving a final design solution.

7. ACKNOWLEDGMENT

This work was supported by a grant of the Romanian Ministry of Research and Innovation, CCCDI – UEFISCDI, project number PN-III-P2-2.1-PED-2019-4375/397/2020 (OnTarget), within PNCDI III.

8. REFERENCES

[1] Hartely-Blossom, Z., et. al. *Microwave Ablation in the Liver: An Update*, Surgical Technology International, vol. 37, pp. 72-78, (2020)

[2] Li, X., Ramadori, P., Pfister, D. *et al., The immunological and metabolic landscape in primary and metastatic liver cancer.* Nat Rev Cancer, Vol. 21, pp. 541–557, (2021).

[3] Vaida, C., Plitea, N., et al., *A new robotic system for minimally invasive treatment of liver tumours*, Proc. Rom. Acad. Ser. A Math. Phys. Tech. Sci. Inf. Sci, vol. 21, pp. 273-280, (2020)

[4] Pisla, D., Gherman, B., Plitea, N., et. al.: *PARASURG hybrid parallel robot for minimally invasive surgery*. Chirurgia, Vol. 106(5), pp. 619-625, 2011

[5] Vaida, C., Pisla, D., Plitea, N., et. al.: *Development of a control system for a parallel robot used in minimally invasive surgery, IFMBE Proceedings*, Vol. 26, pp. 171-176, 2009

[6] Ryder, S.D., *Guidelines for the diagnosis and treatment of hepatocellular carcinoma (HCC) in adults,* Gut 2003;52:iii1-iii8

[7] Sergio, A. et al., *Transcatheter Arterial Chemoembolization (TACE) in Hepatocellular Carcinoma (HCC)*, American Journal of Gastroenterology, Vol. 103, No. 4, pp. 914-921, (2008).

[8] Basri, J.J.A., *et al*., *Robot-assisted radiofrequency ablation of primary and secondary liver tumours: early experience*, interventional, Eur Radiol, Vol., pp. 24:79, (2014).

[9] Basri, J.J.A., *et al*., *Robotic-Assisted Thermal Ablation of Liver Tumours*. Interventional, Eur. Radiol., Vol. 25, pp. 246-257, (2015).

[10] Birlescu, I., Vaida, C., Graur, F., Radu., C., Pisla D., *Medical instrument for robotic assisted radiofrequency liver ablation*, Bulletin of the Transilvania University of Brasov, Vol. 10, No. 2, pp. 1-6, (2017).

[11] Merten, N., Adler, S., Hille, G., et al. *A two-step risk assessment method for radiofrequency ablations of spine metastases*. Comput Biol Med. Vol. 108:174-181, 2019.

[12] Vaida, C., Plitea, N., Gherman, B., Szilaghyi, A., Galdau, B., Cocorean, D., Covaciu, F., Pisla, D. *Structural Analysis and Synthesis of Parallel Robots for Brachytherapy*, New trends in medical and service robot: theory and integrated applications, Mech. Mach. Sci., Vol. 16, pp. 191-204, (2014).

[13] Li, X., Chen, B., et. al. *Transarterial chemoembolization combined with microwave ablation versus microwave ablation only for Barcelona clinic liver cancer Stage B hepatocellular carcinoma: A propensity score matching study*, J. Cancer Res Ther., vol. 16(5), pp. 1027-1037, 2020

[14] Pisla, D., Galdau, B., Covaciu, F., Vaida,C., Popescu, D., Plitea, N. *Safety issues in the development of the experimental model for an innovative medical parallel robot used in brachytherapy*, International Journal of Production Research, Vol. 55 (3), pp. 684-699, (2017)

[15] Liu, P., Qin, J., Duan, B., et al. *Overlapping radiofrequency ablation planning and robot-assisted needle insertion for large liver tumors*. Int J Med Robot. Vol. 15(1):e1952, (2019)

[16] D. Pisla, C. Vaida, I. Birlescu, F. Graur, B. Gherman, P. Tucan, N. Plitea: „Automated medical instrument for radiofrequency ablation" Patent pending: A00379/10.06.2017

O analiză de proiectare funcțională pentru un instrument ghidat robotic utilizat în ablația cu radiofrecvență

Rezumat: *Lucrarea prezintă îmbunătățirea designului unui instrument medical utilizat pentru ablația prin radiofrecvență asistată robotic (RFA). În prima parte, au fost evidențiate cerințele dispozitivului, iar apoi, a fost analizat prototipul dispozitivului și au fost identificate punctele slabe ale acestuia. Au fost realizate unele simulări cu elemente finite pentru a testa rezistența mecanică a dispozitivului în diferite condiții. Pe baza datelor numerice derivate, studiul arată parametrii specifici de optimizare pentru dispozitiv, care pot fi îmbunătățiți fără modificarea structurii sale generale.*

Andrei CĂPRARIU, CESTER, Technical University of Cluj-Napoca, Romania, andreicaprariu@yahoo.com
Nadim Al HAJJAR , Iuliu Hatieganu University of Medicine and Pharmacy, 400000 Cluj-Napoca, Romania, nadim.alhajjar@umfcluj.ro
Calin VAIDA, CESTER, Technical University of Cluj-Napoca, Romania, calin.vaida@mep.utcluj.ro,
Florin GRAUR, Iuliu Hatieganu University of Medicine and Pharmacy, 400000 Cluj-Napoca, Romania, florin.graur@umfcluj.ro
Adrian PÎSLĂ, CESTER, Technical University of Cluj-Napoca, Romania, adrian.pisla@muri.utcluj.ro,
Emil MOIȘ, Iuliu Hatieganu University of Medicine and Pharmacy, 400000 Cluj-Napoca, Romania, emil.mois@umfcluj.ro
Paul TUCAN, CESTER, Technical University of Cluj-Napoca, Romania, paul.tucan@mep.utcluj.ro
Corina RADU, Iuliu Hatieganu University of Medicine and Pharmacy, 400000 Cluj-Napoca, Romania, corina.radu@umfcluj.ro
Iosif BÎRLESCU, CESTER, Technical University of Cluj-Napoca, Romania, iosif.birlescu@mep.utcluj.ro
Doina PÎSLĂ, CESTER, Technical University of Cluj-Napoca, Romania, doina.pisla@mep.utcluj.ro